# FINAL PUBLISHABLE REPORT

| | |
|---|---|
| Grant Agreement number | 18SIB10 |
| Project short name | chipS·CALe |
| Project full title | Self-calibrating photodiodes for the radiometric measurement of fundamental constants |

| | | |
|---|---|---|
| Project start date and duration: | 01.06.2019 (36 + 6 months = 42 months) | |
| Coordinator: *Jarle Gran, Justervesenet* Tel: +47 64 84 84 45 E-mail: jag@justervesenet.no<br>Project website address: http://chipscale.aalto.fi/ | | |
| Internal Funded Partners:<br>1. JV, Norway<br>2. Aalto, Finland<br>3. CMI, Cech Republic<br>4. CNAM, France<br>5. INRiM, Italy<br>6. Metrosert, Estonia<br>7. PTB, Germany<br>8. TUBITAK, Turkey | External Funded Partners:<br>9. IFE, Norway<br>10. SINTEF, Norway<br>11. USN, Norway | Unfunded Partners:<br>- |
| | | |
| RMG01: SFI Davos, Switzerland (Employing organisation); Justervesenet, Norway (Guestworking organisation) | | |

**TABLE OF CONTENTS**

# 1 Overview

*(Please leave this section blank. This section will be completed by the EURAMET MSU using text from the final Publishable Summary.)*

# 2 Need

*(Please leave this section blank. This section will be completed by the EURAMET MSU using text from the final Publishable Summary.)*

# 3 Objectives

*(Please leave this section blank. This section will be completed by the EURAMET MSU using text from the final Publishable Summary.)*

# 4 Results

Radiometric measurements of radiant power at discrete laser wavelengths are possible with cryogenic radiometers (CR) with an uncertainty down to 0.005 %. Cryogenic radiometers are accurate for most applications, but are bulky, expensive and require a high skill level to operate. Dissemination outside discrete wavelengths is carried out with silicon trap detectors and interpolation functions. The trap detectors' properties and insufficient stability is limiting the comparison agreement at the NMI level to a spectrally dependent dispersion around 0.1 %. Existing measurement techniques are not suitable for miniaturisation and providing traceability to integrated measurement systems, which is the direction technology development are moving.

The overall objective of the chipS·CALe project is to develop improved photodiodes, new instrumentation and measurement techniques as a self-calibrating photodiode. This is achieved by targeting the objectives by developing improved modelling of photodiodes and using the knowledge to develop improved photodiodes. Furthermore, project objectives were to develop the packaging technology and instrumentation to calibrate the photodiodes directly linked to electrical power measurement (electrical substitution) and to demonstrate the measurement capability in the exploitation of them.

### Objective 1:

*To develop improved and validated 3D charge-transfer models to predict the PQED internal quantum deficiency. The target prediction uncertainty is a relative uncertainty of 10 % of the internal quantum deficiency value for high values and an absolute uncertainty of 10 ppm of the internal quantum deficiency for values below 100 ppm.*

The purpose of the objective is to exploit the Predictable Quantum Efficient Detector (PQED) developed in this project to provide improved and simplified traceability in the 400 nm to 850 nm range. To do so we developed for the first time a Digital Twin of the PQED as a 3D charge carrier simulation model and used it to

I. improve the uncertainty in the responsivity to go beyond the IQD losses and
II. independently extract the photodiode model parameters.

In this way, 3D models were used to put intelligence into the measurement system providing improved understanding and enabling new measurement techniques to be developed and applied. The PQED Digital Twin was developed to mimic the real physical PQED and the observed properties of the actual PQED was used as a reference to the digital version. Figure 1-1 shows an illustration of a 7-reflection PQED.

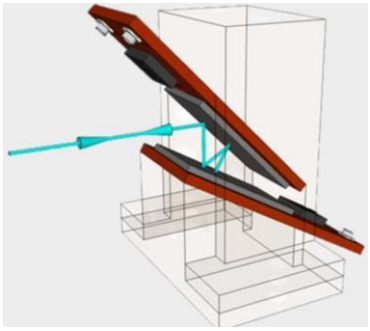

**Figure 1-1**. Illustration of a 7-reflection Predictable Quantum Efficient Detector (PQED) consisting of two induced junction photodiodes.

### Initial modelling

At the beginning of the project, before photodiodes produced in chipS·CALe were available, a simplified 3D simulation model was developed based on the known structure of the actual photodiodes developed in the qu-candela project. Preliminary simulations had been made and revealed that when simulating internal losses as a function of bias voltage at various power levels, the influence of total losses was dependent on five physical parameters. Those parameters were bulk doping, fixed oxide charge, bulk lifetime, surface recombination parameter and beam size. The simulations also revealed that each of the model parameters affected the total losses differently and with different weight at various power levels. The four first parameters are properties defining the structure of the photodiode and the beam size is a feature of the experiment. These findings laid foundations for a proposed new experimental method to provide traceability; how can we exploit the predictability of the Digital Twin to mimic and extract the actual physical properties of the photodiodes. In order to succeed, an experimental approximation of the internal losses had to be found. We knew that the PQED type photodiodes are expected to have very low losses. This means that measuring the photocurrent (I) as a function of bias voltage (V) and displaying the result as the relative change in current against the maximum current value will directly be an approximation of the internal quantum deficiency (IQD) as a function of bias voltage, assuming that the maximum photocurrent value represents zero internal losses. With the same measure represented experimentally and by simulation, fitting the model to multiple curves simultaneously would reveal the actual physical properties of the photodiodes.

### Fitting of simulation model to experimental I-V curves

Fitting was done to several I-V measurement curves of three different PQED trap detectors at 476nm, 488 nm and 647 nm using one unique set of parameters for each PQED. Each I-V set consists of up to five different power levels between 100 µW and 1000 µW and have been produced by two different laboratories. In the measured change in photocurrent with bias voltage, the IQD vary several orders of magnitude from tens of percent to tens of ppm depending on optical power, bias voltage and beam size. The curves are shown in figure 1-2(a). The software we used, Genius device simulator from Cogenda, did not have the ability to make simulations with a gaussian beam profile. This meant that a cylindrical beam approximated to the gaussian beam had to be developed, as illustrated in figure 1-2(b). We chose an approximation where the peak intensity of the gaussian beam matched the height of the cylindrical approximation and the radius of the cylinder was adjusted so that the volume of the gaussian and cylinder were the same.

As seen from Fig 1-2(a), the internal losses of the PQED are much higher for high power levels than lower power levels. The first photodiode absorbs most of the power and will therefore contribute more to the losses seen in the experiment. In order to achieve a power level representative for the actual measurement, we assumed that all losses are from the first photodiode. At the wavelength of 488 nm with a standard PQED from the qu-candela project, 86 % of the current is produced by the first photodiode. In the IQD model fitting we therefore used 86% of the power applied in the experiment.

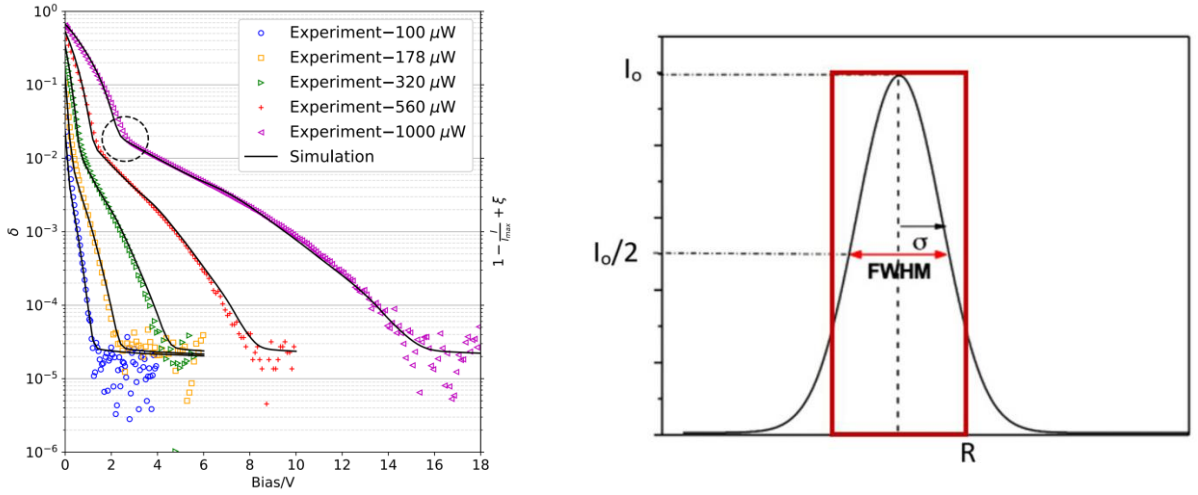


(a) (b)

**Figure 1-2**. Relative change in photocurrent to maximum photocurrent value is shown with fitted IQD model by varying four photodiode defining parameters (a). A 2D projection of the cylindrical beam approximation to a gaussian beam used in the fitting is shown in (b), where $R = \sqrt{2}\sigma$.

Furthermore, to reduce the computation time of the software, a simplification in the simulation structure was necessary. The actual physical dimensions of the PQED photodiodes are quite large (11x22 mm$^2$) which requires a large number of mesh nodes. We therefore used a simulation structure as shown in Fig 1-3.

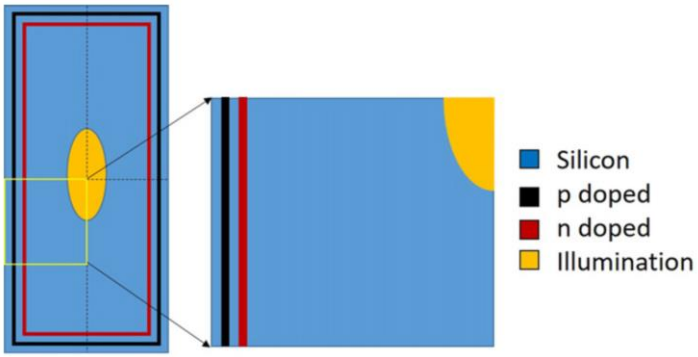


**Figure 1-3**. Simplified simulation structure (to the right) used in the initial simulation fit to qu-candela photodiodes.

A remarkably good fit of the predicted IQD to the relative photocurrent measurement at different power levels and bias voltages was achieved despite the simplified 3D simulation model used, as seen in Fig. 1-2 (a). The excellent fit shows that the Digital Twin model describes very well the performance of the photodiode and demonstrates that a very good understanding of the physics of the device is achieved. The fits are based on parameters that describe the properties of the photodiode. Once these parameters are known, prediction of the responsivity at any wavelength can be made. This shows that measurements at one wavelength only is sufficient to predict the responsivity over a wide spectral range. This approach not only simplifies the traceability, but produces results with far lower uncertainty as well. A paper describing the method was published in Metrologia (https://doi.org/10.1088/1681-7575/ac604b).

### Temporal stability

Since the manufacturing of the first PQEDs in the qu-candela project, measurements of their responsivity have been made at PTB and CMI against their cryogenic radiometer. Both PTB and CMI were unable to detect any drift of this type of detector over more than a decade to the uncertainty level of the technique. This feature is making the PQED an excellent carrier of a spectral response scale, as it turns out that the calibration interval

of these detectors can be long. This means that the physical properties of the PQED are maintained and that the responsivity limiting properties like SRV parameter and fixed oxide charge, must be maintained over time. A comparison between the PQED stability and typical drift curves for the commonly used Hamamatsu S1337-1010 is shown in Fig. 1-4.

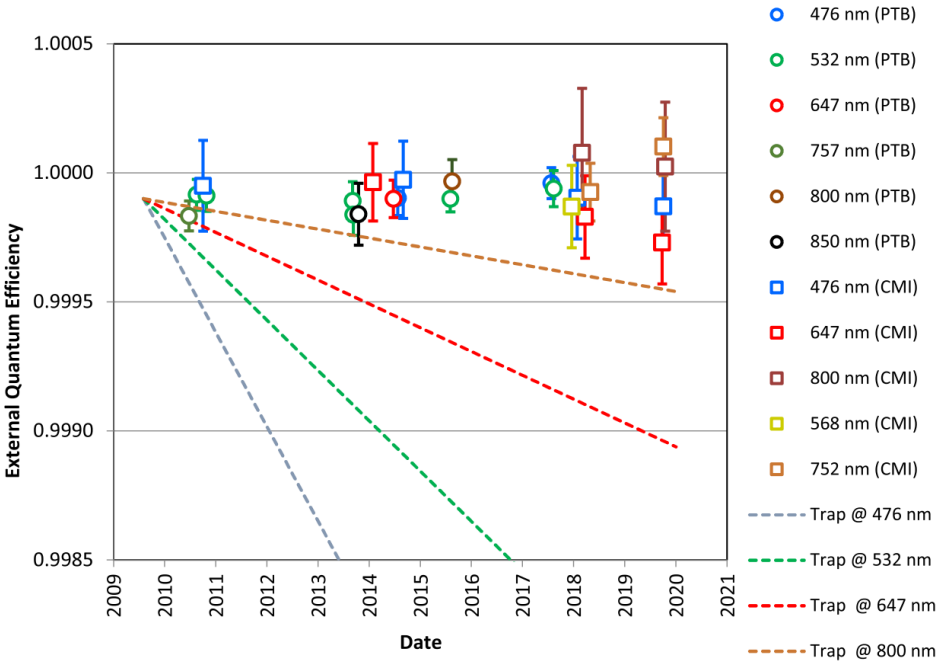


**Figure 1-4**. Comparison between external quantum efficiency of PQEDs and typical spectrally dependent drift curves of the commonly used Hamamatsu S1337-1010 trap.

### Quantum yield

The work on limitations in PQED prediction uncertainty has revealed that quantum yield (or gain) has to be taken into account for wavelengths below 450 nm for high accuracy applications better than 200 ppm. Despite measuring on two PQEDs with different IQD, as seen in Fig. 1-5(a), they both produced the same yield value when correcting for the individual differences in IQD, as seen in Fig. 1-5(b). It was demonstrated by Metrosert that the yield can be modelled with an agreement to measurements of around 100 ppm from 400 nm to 450 nm and hence predictability in the PQEDs response is maintained down to 400 nm by post processing the IQD. This mean that we have a fully predictable detector at least from 400 nm to 850 nm.

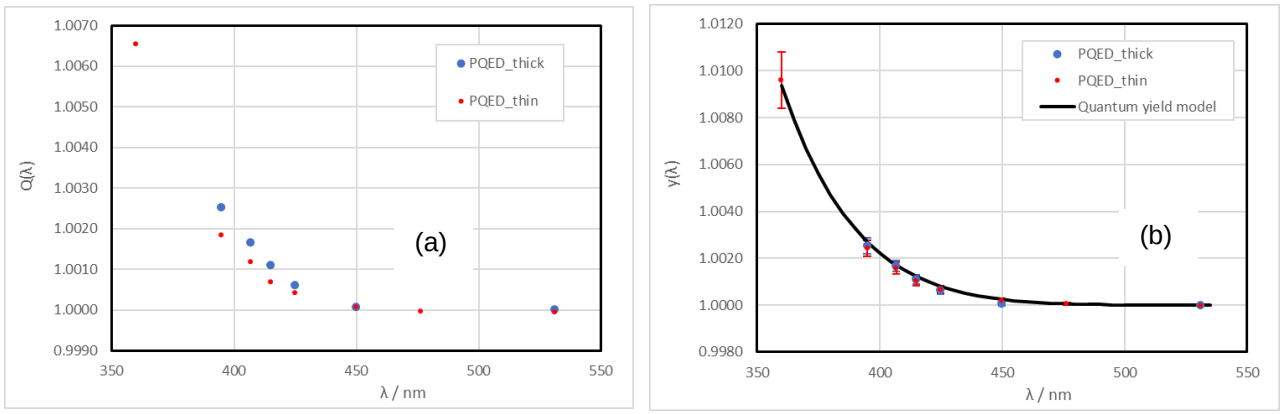


**Figure 1-5**. Measured external quantum efficiency of two PQEDs are shown (a). Subtracting the modelled internal quantum efficiency and reflectance gives the true quantum yield (b). The quantum yield can be modelled as shown with the solid line.

### IQD at cryogenic temperatures

The performance of PQEDs as a function of temperature can be predicted by its Digital Twin. The simulated 1000 µW IQD curve in Fig. 1-2 (a) is displayed for different temperatures in Fig. 1-6. It reveals that the linearity of the PQED should improve with reduced temperature and internal quantum deficiency should be smaller at reduced temperatures when sufficiently biased at visible wavelengths.

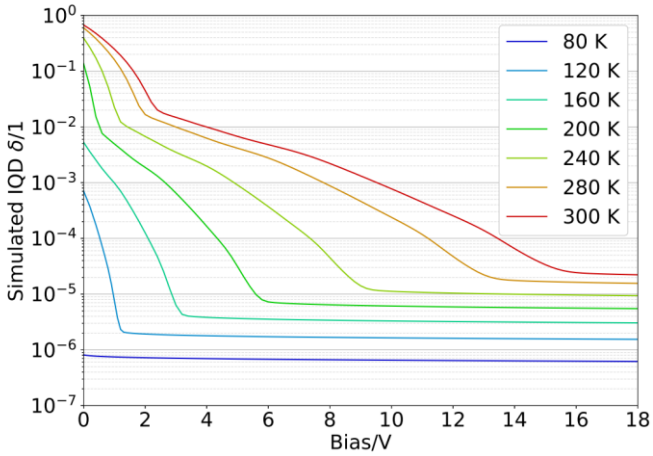


**Figure 1-6**. The predicted IQD of the PQED as a function of temperature and bias voltage by its Digital Twin.

In chipS·CALe we also developed and manufactured improved PQED photodiodes with lower internal quantum deficiency. How this was achieved, and their characteristics will be highlighted in the chapter concerning objective 2. Due to their characteristics, the former simulation model was not able to produce losses low enough to match the actual (I-V) measurements of the PQEDs. A full structure of the photodiode had to be developed with a finer mesh and larger area as shown in Fig 1-7 (a). It has been shown that the chipS·CALe PQEDs have better performance with different parameters than previous PQEDs.

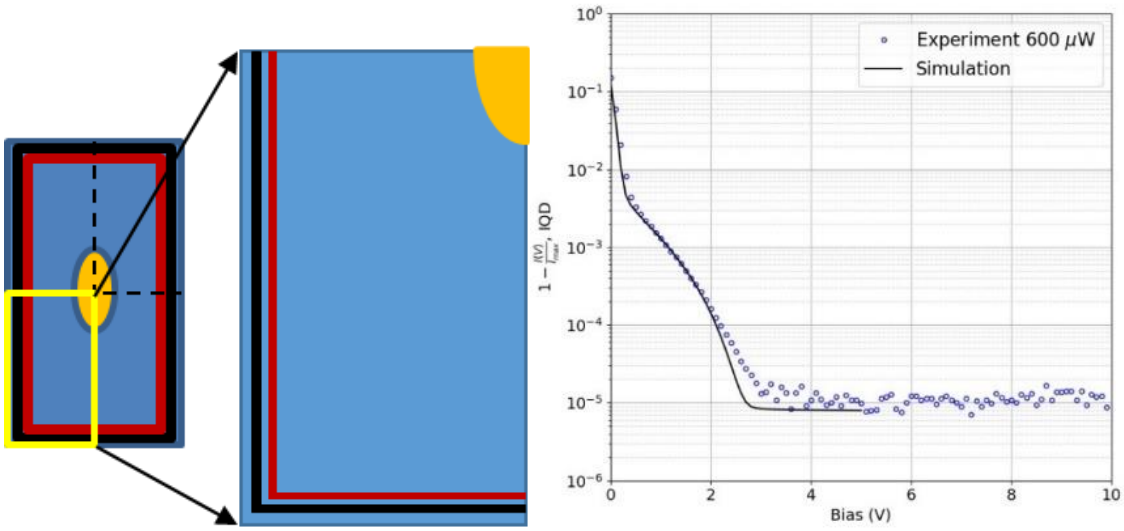


(a) (b)

**Figure 1-7**. Visualisation of the simulation model used for chipS·CALe photodiodes (a). The comparison between the experimental approximation curves and predicted IQD with parameters from manufacturing are shown (b).

**Pushing the limits of the state-of-the-art**

Extensive characterisations and validations at room and cryogenic temperature have shown that the chipS·CALe PQEDs have better performance than previously developed PQEDs. There is a very good agreement between the modelled properties of the PQED provided by its Digital Twin and actual measurements at various temperatures. These results show that we expect the PQED to work with better linearity, and hence at higher power levels, when cooling the detector to cryogenic temperatures for wavelength up to 760 nm. For longer wavelengths the picture is more complex as the reduced absorption coefficient causes photons to penetrate beyond the depth of the photodiode. At room temperature, the total losses of the PQED, including internal losses, reflectance, potential absorption and scatter, was confirmed to be as low as 10 ppm (with 30 ppm uncertainty), hence stretching the limits of the cryogenic radiometer. This is two orders of magnitude better than world-wide commonly used transfer standard detectors from Hamamatsu. However, we had to improve the Digital Twin to accurately describe the properties of the new PQED, which led to a significantly extended computational time. Reducing the computational time and improving model accuracy is a task for the future.

**Summary**

The objective was successfully met thanks to the improved 3D modelling by JV combined with Metrosert's post-correction quantum yield model. The predictable spectral response of the PQED as an independent measurement standard was demonstrated by fitting the losses to an experimental representation of the internal quantum deficiency at one wavelength only. This means that measurements at one wavelength only is sufficient to predict the responsivity over a wide spectral range. A state-of-the-art characterisation capability and shared work between Aalto, CMI and PTB have revealed similar and reproducible results between different laboratories. Extensive and challenging validations have been conducted by PTB and CMI which confirms the capabilities of the models to the uncertainty level of their primary standard.

## Objective 2:

*To develop the best possible PQED photodiodes for cryogenic operation by using the improved 3D models and evaluation of passivation layer materials, passivation strategies and charge increasing techniques. To manufacture a batch of optimised PQED photodiodes and to acquire bare-chip photodiodes for room temperature operation*

The development of the optimised PQED was a joint effort based on JV's Digital Twin photodiode, SINTEF's process and detector manufacturing facilities, IFE's lifetime characterisations, INRIM's refractive index measurements and USN's expertise in packaging.

### Optimising the passivation recipe

Photodiodes with excellent and record low external quantum deficiency were successfully manufactured in chipS·CALe and have thereby reached the most important goal of this project. Different passivation materials ($SiO_2$, $SiN_x$ and $Al_2O_3$) were studied. Surface recombination velocity and fixed oxide charge are, based on simulations, highlighted as the key parameters for optimising PQED photodiode properties. Simulations were the key to success in the manufacturing of improved photodiodes, because the problem narrows down to how well the passivation of the surface of the photodiodes can be made. This means that we could evaluate how well different passivation recipes work with very few process steps and simple and quick standard characterisation methods. Based on the outcome of the characterisations, surface recombination, bulk lifetime and fixed charge are extracted, and the expected responsivity of a photodiode can be predicted without going through costly process steps, challenging and time-consuming characterisations.

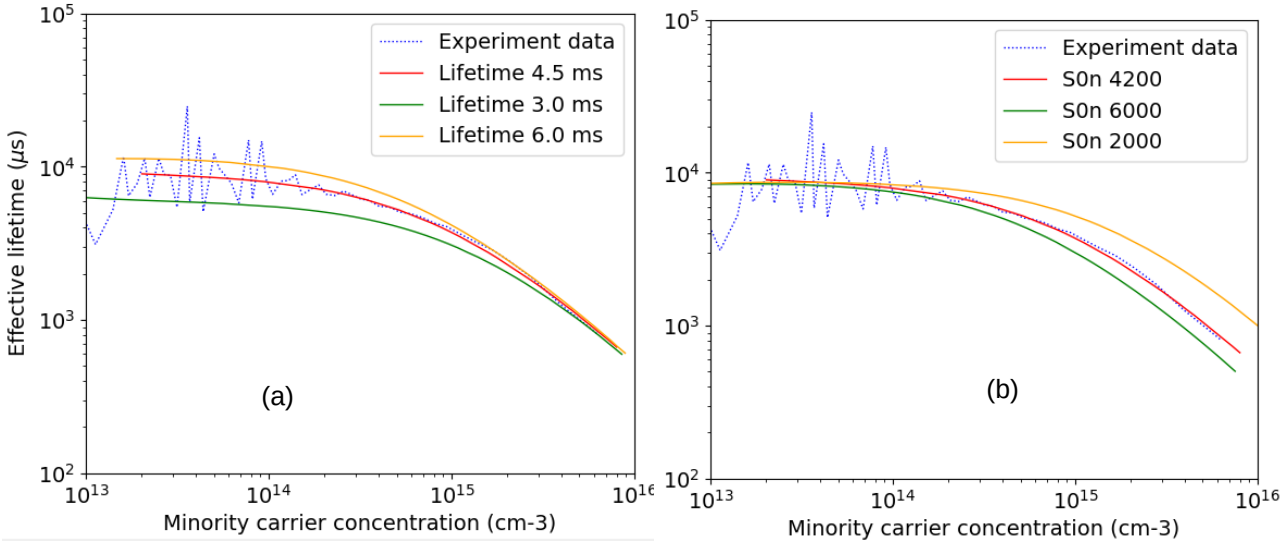


**Figure 2-1**. The sensitivity of bulk lifetime (a) and surface recombination velocity (b) on the effective lifetime measurement curve as a function of minority carrier concentration.

Having excellent charge carrier passivation is not sufficient and other parameters like non-uniformity and absorption must also be avoided. Different deposition recipes were tested and varied in several rounds by SINTEF and various characterisations were made. IFE measured the effective lifetime by two different techniques and JV simulated the lifetime recombination and separated the two recombination parameters from the measurements. The sensitivity of bulk lifetime and surface recombination velocity on the effective lifetime curve are shown in Fig. 2-1. The lifetime technique is a sensitive technique that extracts the essential parameters and predicts expected losses from a photodiode if manufactured by the recipe.

### Reducing reflectance losses

Additional to the charge carrier optimisation, the optical quality and uniformity in the process had to be monitored. For the most promising recipes, INRIM measured the refractive indices and potential absorption in the passivation layer over the whole spectral response range from 400 nm to 850 nm. An example of this is shown in Fig. 2-2, with an illustration of a 7-reflection trap. In addition to look for absorption, the data quantified the refractive indices which were used to tune the process so that minimum reflectance over the full spectral range could be achieved.

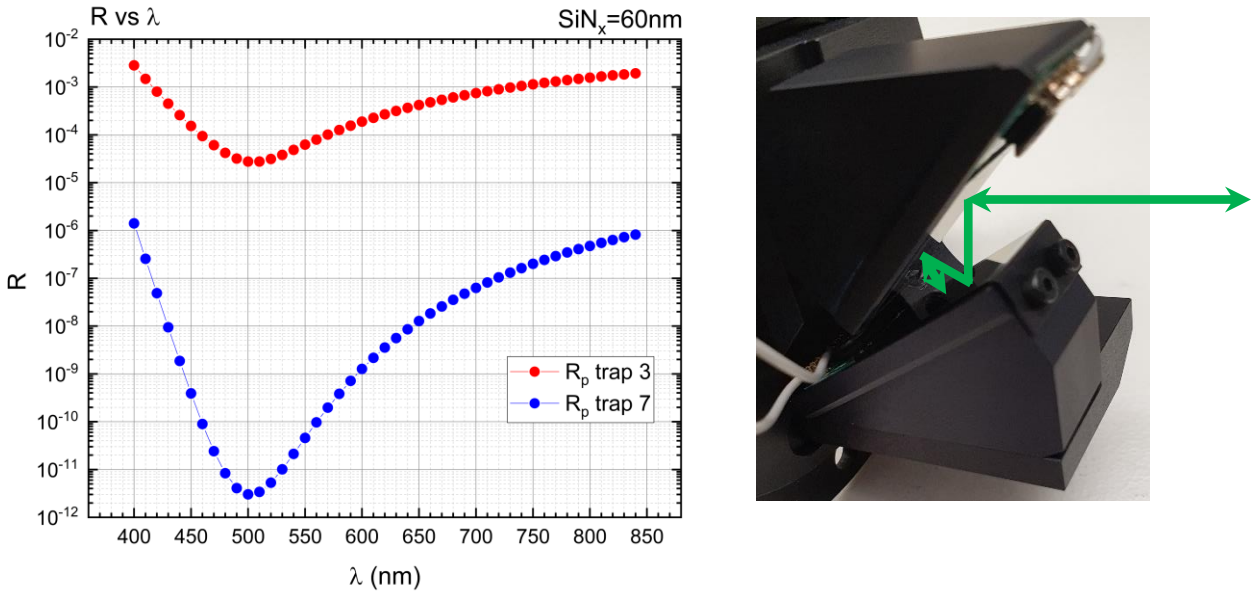


**Figure 2-2**. Calculation of reflectance from measured refractive indices at optimised thickness (left) if mounted in a wedge trap configuration with 3 or 7 reflections (right).

The $SiN_x$ passivation process recipe without any optical absorption and with fixed oxide charge 2-5 times higher than well working qu-candela photodiodes was achieved.

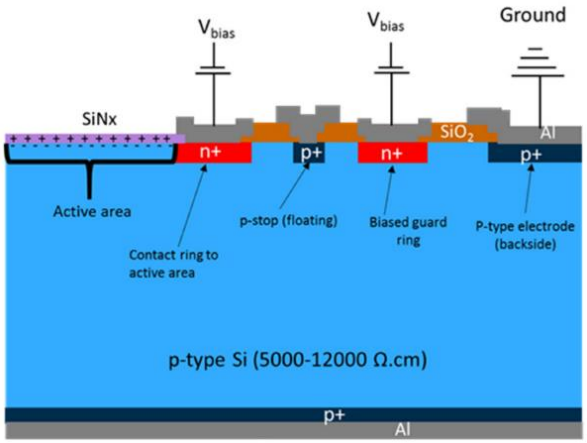


**Figure 2-3**. Inversion layer photodiode structure and biasing scheme. The n+ and p+ regions, formed by phosphorous implantation and boron implantation, respectively, have peak doping concentrations of $>10^{19}$ $cm^{-3}$ and profile depths of ~2 µm.

Measurements of their responsivity show that the photodiodes manufactured in chipS·CALe are the best for calibration purposes ever produced. High fixed charge improves the linearity of the photodiodes and enables the dual-mode techniques to be exploited at higher power and thereby with better signal to noise ratio (SNR). A batch of $Al_2O_3$ photodiodes is also completed.

### Lifetime measurements and IQD prediction

Thanks to improved 2D and 3D simulation models, one can predict the photo response of an inversion layer photodiode made with surface passivation materials of given specific properties. The predictability of response through accurate modelling by the Digital Twin is not only essential for the use of the photodiodes as a primary standard, but also allows one to optimize the passivation to improve the quantum efficiency of the detector without having to go through costly full fabrication of photodiodes and time-consuming and insufficient characterisations of the photodiodes.

From lifetime measurements, prediction of the expected photodiode responsivity, if they were manufactured with the various passivation layers, was done. This is shown in Fig. 2-4. This demonstrates a new independent measurement technique of the photodiode responsivity from material characterisations and simulations only. At room temperature, the predicted IQD around 1 -10 ppm and 10-100 ppm of the two produced photodiode types are consistent with the measurements of photocurrent ratios between cryogenic radiometers and chipS·CALe PQEDs. Uncertainties and IQD variations in the 1-10 ppm range, as displayed here, are beyond the capabilities of current state-of-the-art by an order of magnitude and would probably not be able to characterise detectors with sufficient uncertainty, even in relative measurements.

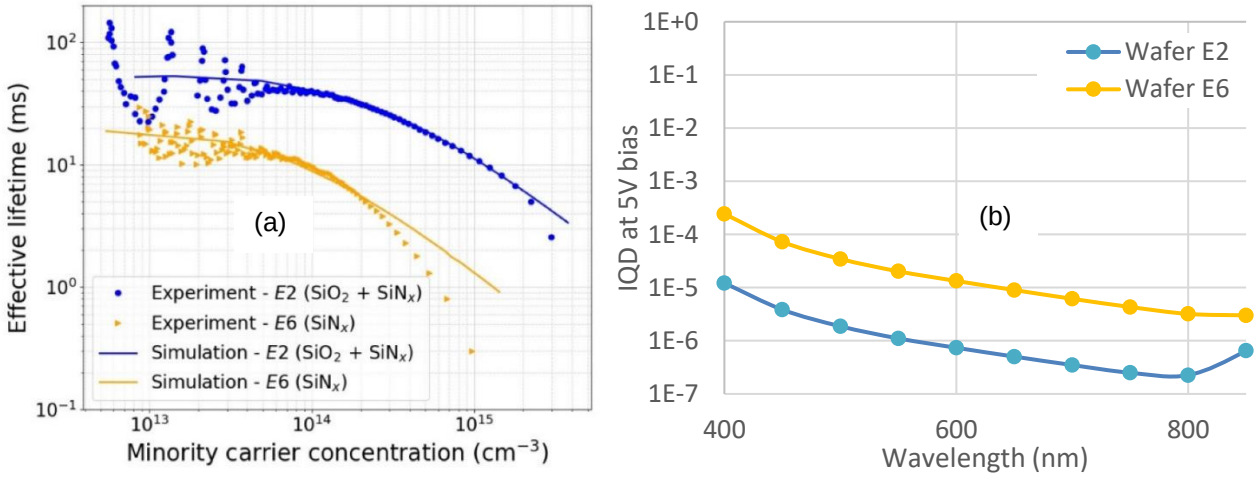


**Figure 2-4**. Lifetime measurements of two passivation processes based on purely SiNx (yellow) and a stack of SiO2 and SiNx (blue) including lifetime fitting (solid lines) is shown in (a). The expected internal quantum deficiency if a photodiode was manufactured by this recipe is shown in (b).

### Characterisation of optimised photodiodes

Various characterisations of the manufactured PQED photodiodes were done by project partners PTB, CMI, INRIM and Aalto. The characterisations consisted of I-V measurements, linearity, uniformity and measurements against other primary standards as the cryogenic radiometer and qu-candela PQEDs.

When comparing the photocurrent measurements between chipS·CALe photodiodes and the qu-candela photodiodes, as seen in Fig. 2.-5, it is evident that we have a more defined bend in the curves for chipS·CALe photodiodes around 2 V. This is caused by the higher fixed charge in chipS·CALe photodiodes. Furthermore, the amplitude of the curve to the right of the 2V bend is lower for chipS·CALe photodiodes than for qu-candela photodiodes, showing that the surface recombination velocity is lower for chipS·CALe photodiodes. These experimental results support the predictions made by the Digital Twin from the C-V and lifetime measurements in the material characterisations comparing the results from Fig. 2-4 and Fig. 1-7. There are therefore agreement between the two independent realisations based on the Digital Twin PQED, but potential non-accounted error sources may be present.

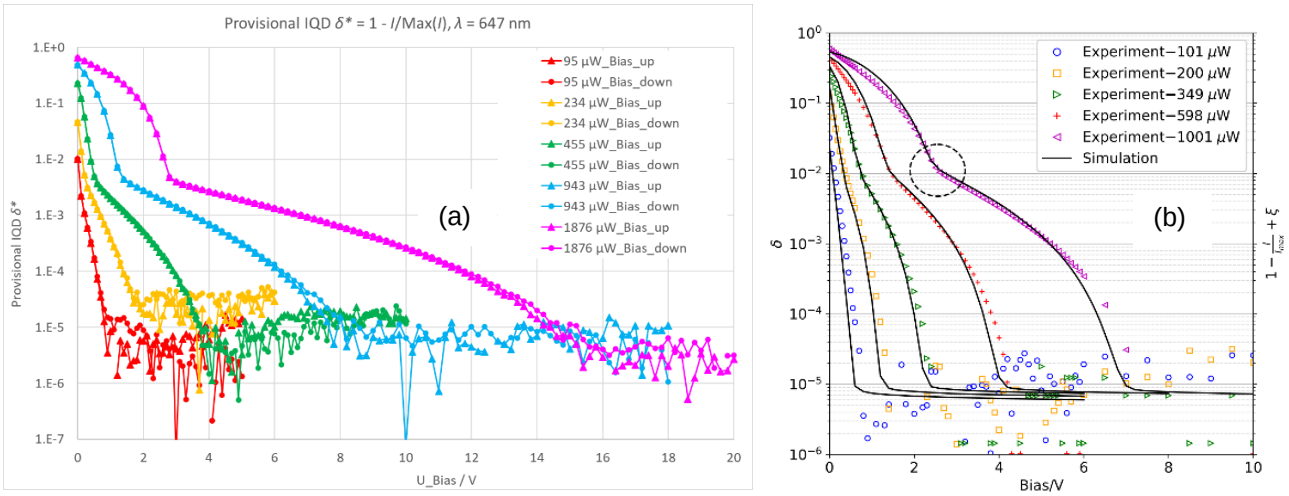


**Figure 2-5**. Comparison between I-V measured curves at 647 nm of chipS·CALe photodiodes (a) and qu-candela photodiodes (b).

The measured non-uniformity of the PQEDs in a trap structure was limited by the stability of the laser beam and was between 4 ppm to 30 ppm of the central 2 mm x 2 mm. The photodiodes were proven to be linear to at least 2 mW at room temperature when sufficiently biased.

**Lifetime measurements at low temperature**

A set-up making charge carrier lifetime measurements from 80 K to 300 K has been successfully developed by IFE and used to evaluate different process test samples. To the best of the consortium's knowledge, this is the first time lifetime measurements over such large temperature range has been performed. Simulation models were used to separate bulk lifetime and surface recombination velocity from the lifetime measurement. Unfortunately, the lifetime is reduced on all test samples when reducing the temperature. This means that photodiode parameters are changing with temperature and the expected reduction of losses at low temperature will not be fully achieved.

Characterisations of the photocurrent as a function of bias voltage at cryogenic temperatures given in Fig. 2-6 shows that the simulation predictions given in Fig.1-6 are confirmed. The photodiode linearity improves significantly and almost no bias voltage is required to achieve full saturation even at 1 mW.

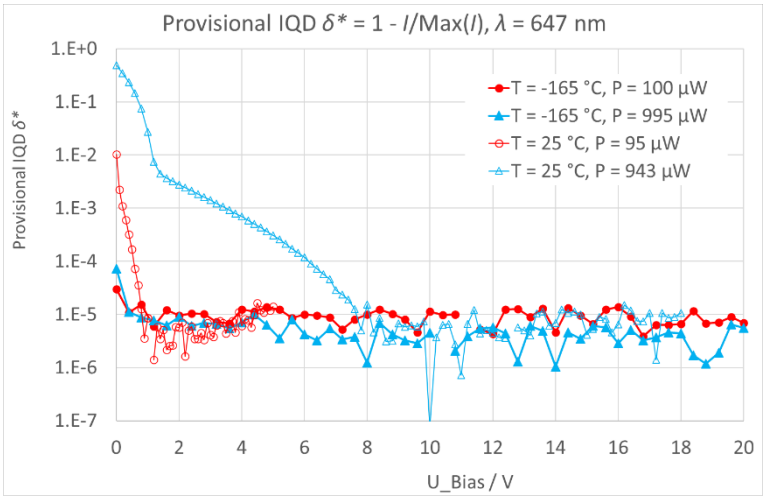


**Figure 2-6**. Comparison of I-V measurements at room temperature and cryogenic temperature.

Photodiodes need to be packaged in a way such that the current can be effectively read, mounted in a mechanical structure and allowing measurements over a wide temperature range without breaking due to thermal strain. The solution was to use a custom-made silicon substrate as a carrier and glue the photodiode to the substrate with a thin and controlled layer of low viscosity glue resulting in a parallel mounting between the photodiode and carrier. Parallel mounting of the photodiodes is important for achieving the correct angle between photodiodes when mounting them in the mechanical trap structure. Convenient U.FL connectors were used to couple the device to an external circuit. As the connector is hard to fix to the silicon carrier a PCB is used as a hub for connector, wire bond and washer for the hole to fix the detector carrier to the trap mechanics.

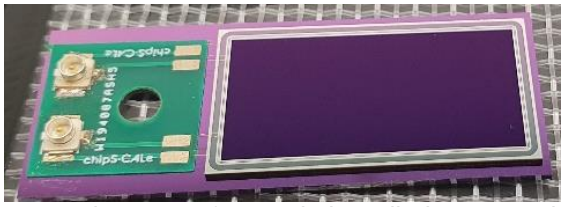


**Figure 2-7**. Photo of the complete manufactured photodiode mounted on the chip carrier.

Validations of the PQED were made with measurements of optical power against the cryogenic radiometers at CMI and PTB. In addition, measurements against PQEDs from previous projects were made by Aalto. Those calibrations showed that a deviation in the 10 ppm range between the chipS·CALe PQEDs and the best cryogenic radiometers made is achieved. These results confirm the excellent properties of the PQEDs. The agreement was limited by uncertainties in the technique of 30 ppm.

The excellent quality of the manufactured photodiodes reduces the need for accurate prediction of the EQD value. Our examinations indicate that responsivity of these photodiodes mounted in a 7-reflection trap structure deviates in the 1 ppm range from an ideal photodiode whose responsivity is given by fundamental constants and the applied wavelength only.

**Summary**

The joint effort and individual expertise by different partners were combined and resulted in the great achievement of producing photodiodes with record low internal and external losses. The work towards improved PQED photodiodes is published in Sensors 2021, 21, 7807 (https://doi.org/10.3390/s21237807). Thanks to modelling, prediction of the expected responsivity of a photodiode could be made based on the properties of the deposition recipe. Fast lifetime characterisations were used to extract the parameters defining the performance of the PQED photodiodes. In this way, many generations of deposition recipes could be tested without going through a full manufacturing round and time-consuming device characterisations to evaluate the best passivation recipe. Thorough characterisation and validations confirm that the photodiodes developed in chipS·CALe have the lowest internal and external losses the consortium partners are aware of when mounted in a trap configuration. The validations also support the predictions by the 3D simulation model. The objective was successfully met.

## Objective 3:

*To develop instrumentation and packaging enabling self-calibration of photodiodes. The photodiodes should be operated in both photocurrent and electrical substitution mode with sufficient sensitivity and equivalence between optical and electrical heating over a temperature range from 20 K to 300 K.*

The purpose of this objective was to develop the technology enabling optical power measurements using electrical substitution on silicon photodiodes, to allow dual-mode operation of the photodiodes. Packaged devices for both room temperature and cryogenic temperatures were developed based on thermal simulation models with COMSOL Multiphysics.

During electrical substitution of the dual-mode device, the device is heated both optically and electrically. The optical heating of the photodiode is made in the position of the beam spot, usually in the centre of the photodiode. Electrical heating is done by forward biasing the photodiode, such that the heat is deposited around the edges of the photodiode. This difference in heating profiles between optical and electrical heating causes a challenge, as the electrical substitution method requires equal temperature rise at the position of the temperature sensor from equal amounts of optical and electrical power. The dual-mode detector design was thus developed and optimised with the aim of reducing this thermal non-equivalence to a minimum. With the final design achieved in the project, the thermal simulations show that heat equivalence meeting the target uncertainties, 0.05 % at room temperature and 1 ppm at cryogenic temperature, is achievable.

### Self-calibration of photodiodes – the dual-mode detector

The dual-mode detector (DMD) is a photodiode assembly which incorporates both a photodiode and a temperature sensor, as well as thermal interface materials and electrical connections, and packaged in such a way that it can be operated in two modes:

- *Photocurrent mode*, in which the absorbed power is measured by the photocurrent and
- *Thermal mode / Electrical substitution mode,* in which heating caused by absorbed optical power is compared to heating from a known electrical power.

The thermal mode can be used as a reference to calibrate the spectrally dependent internal losses $\delta(\lambda)$ of the photodiode, in what we call a self-calibration measurement, by combining the results of the two modes, in the following way:

$$\delta(\lambda) = 1 - \frac{i_{photo}}{P_{opt}} \cdot \frac{hc}{e\lambda} \tag{3-1}$$

where $i_{photo}$ is the measured photocurrent, $\lambda$ is the wavelength of the incoming radiation, $c$ is the vacuum speed of light, $h$ is Planck's constant and $e$ is the elementary charge. The absorbed optical power determined from thermal mode, $P_{opt}$, is estimated from the equivalent thermal response with electrical power, $P_{el} = VI$. Here $V$ is the measured voltage across the photodiode and $I$ is the measured current through the photodiode. By heating the detector module at two different levels of electrical power, one slightly above and one slightly below the optical power level, the optical power can then be found from a linear fit based on the two electrical levels.

The thermal non-equivalence $\gamma$, caused by the difference in temperature profiles between electrical and optical heating, is defined as

$$\gamma = \frac{R_{th,opt} - R_{th,el}}{R_{th,el}} \tag{3-2}$$

where $R$ is the thermal responsivity ($R = \Delta T/P$ ). This non-equivalence leads to an error in the measured IQD that must be accounted for.

Objective 3 involved designing packaging that minimised the non-equivalence, with targets being below 500 ppm at room temperature (RT) and below 1 ppm at cryogenic temperature (CT).

### Modelling and simulation of dual-mode detectors

COMSOL Multiphysics was used by USN, with input from JV, Metrosert and INRIM, to simulate the thermal behaviour of the detector module and develop the DMD designs. Thermal solid conductance and thermal emission were considered as the dominant heat transfer mechanisms, while thermal convection was ignored due to the vacuum pressure during operation.

It was found that for room temperature operation, thermal emission was a significant contribution to heat dissipation and thereby non-equivalence. Thus, the actual emissivity of the photodiode front side was an important parameter in determining the non-equivalence. The emissivity of the produced photodiodes was measured using a FTIR spectrometer by PTB, and the measured value was used in the simulation model.

**Thermal design**

Two designs for packaging of DMD modules were developed:

- *DMD-v1* was built using a simple structure with a silicon thermal diffuser bonded on the short side of the photodiode. It was electrically heated using forward biasing of the photodiode and was designed for use at both RT and CT.
- *DMD-v2* was developed to reduce the effect of thermal emission at room temperature by using a more symmetric structure and was electrically heated using a backside mounted custom designed heater.

*DMD-v1*

The structure of *DMD-v1* is shown in Fig. 3-1(a). The photodiode was bonded to a thermal diffuser made from epoxy and silicon, which in turn was bonded to a thin PCB with an attached temperature sensor. An aerogel spacer was used to limit the heat flow directly to the copper heat sink. The time constant and thermal responsivity was tuned by designing the thermal resistance of the weak link, which is partly defined by the dimensions of the copper tracks connecting the photodiode to the copper heat sink, seen in Fig. 3-1(b).

Two versions of DMD-v1 were designed and fabricated – one for room temperature and one for cryogenic temperature, where the difference was the type of temperature sensor and the weak link. For the RT version, Semitec (Mfr. No: 103FT1005A5P1) temperature sensors were used, while for the CT version, Cernox temperature sensors were used. In the CT version, the thermal resistance of the weak link was increased by increasing the length and decreasing the widths of the copper tracks (Fig. 3-1(b)) compared to the RT version.

Figure 3-1(c,d) shows the simulated non-equivalence at RT and 40 K, respectively. At RT there is a dependence on beam alignment in the non-equivalence of 280 ppm/mm, which is due to the thermal emission. The slope of 280 ppm / mm displacement was confirmed with low noise electrical substitution measurements (https://doi.org/10.1088/1681-7575/ac6a94).

At 40 K, the thermal non-equivalence is well below 1 ppm. Figures 3-1(e,f) show the predicted time constant and thermal responsivity between 25 K and 290 K. When lowering the temperature, the responsivity initially increases due to the reduced thermal emission, before decreasing due to the increase thermal conductivity of copper at cryogenic temperatures.

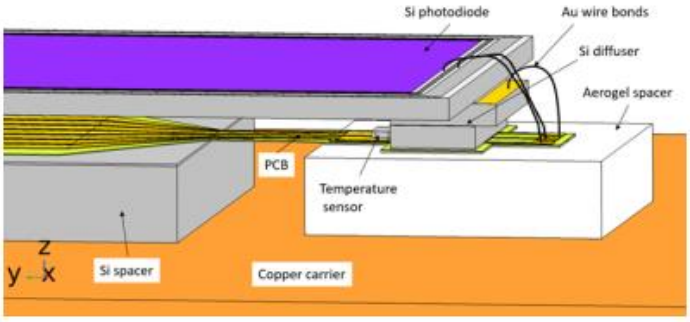


(a)

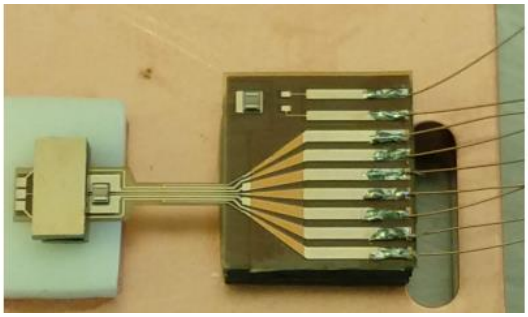

(b)

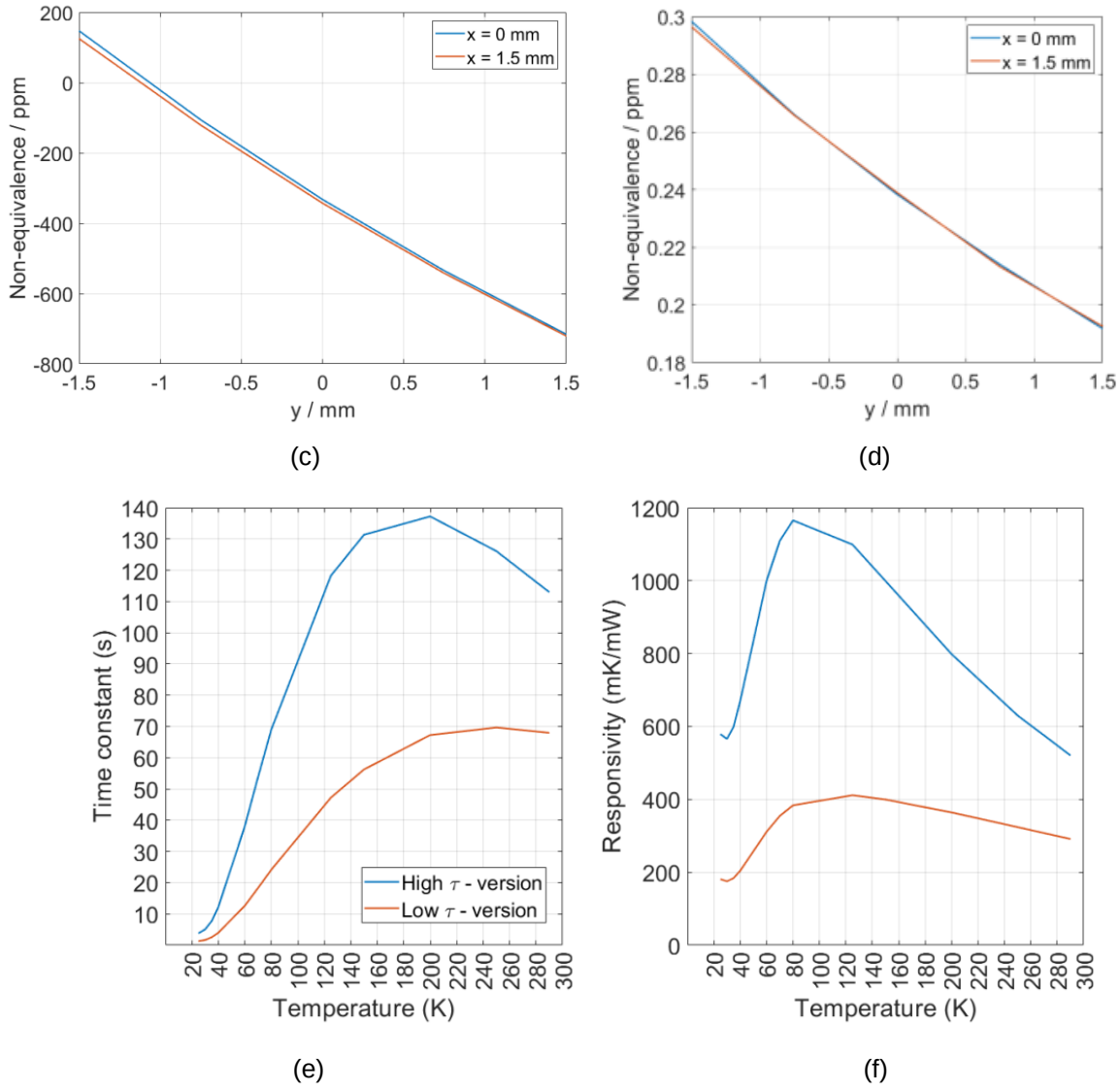


**Figure 3-1**. (a) Model of the DMD-v1 module. (b) Fabricated DMD-v1 structure (CT version) before photodiode mounting. (c,d): Simulated non-equivalence as a function of beam misalignment (x,y) for 1 mm beam radius at (c) 290 K (low $\tau$-version) and (d) 40 K (high $\tau$-version). Simulated time constant (e) and responsivity (f) for high and low time constant ($\tau$) versions.

*DMD-v2*

The structure of DMD-v2 is shown in Fig. 3-2(a). The photodiode was bonded to four silicon “legs” in a symmetric structure, as seen in Fig. 3-2(b), and had a thin heater adhesively bonded to the backside and connected to a PCB also glued to the backside. The four legs were in turn bonded to a second PCB with an attached temperature sensor. The simulated non-equivalence was below 100 ppm for misalignments up to 1.5 mm in one direction, as shown in Fig. 3-2(d). Compared to DMD-v1, the better non-equivalence of DMD-v2 comes at the expense of a higher time-constant, as shown in Fig. 3-3. DMD-v1 has a predicted time constant close to the “ideal” value, corresponding to the heat capacity of the photodiode.

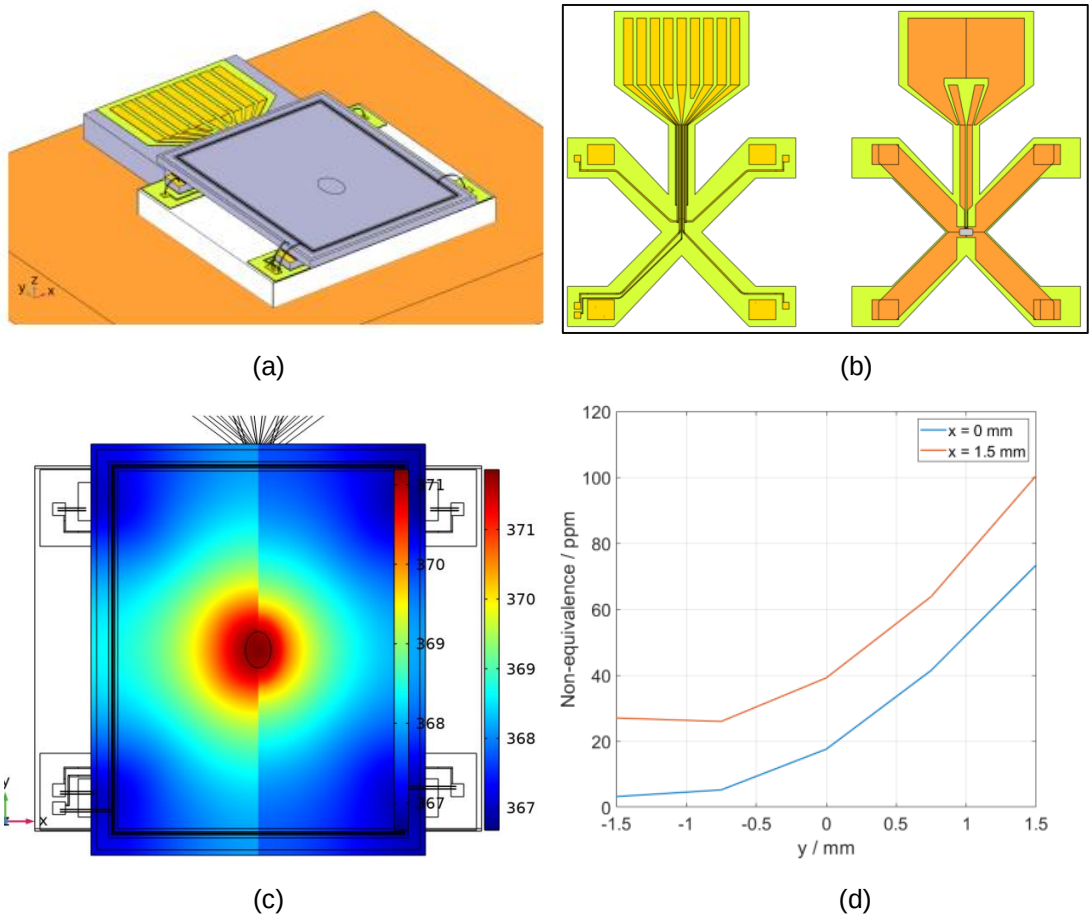


**Figure 3-2**. (a) Overview of assembled model DMD-v2. (b) Model of the PCB (front and backside) with attached temperature sensor on the backside. (c) Split figure of simulated temperature distribution (ΔT in mK) on photodiode surface for electrical heating using backside heater (left side) and optical heating with beam incident on center of photodiode (right side) at room temperature. (d) Simulated non-equivalence as a function of beam misalignment (x,y) for DMD-v2.

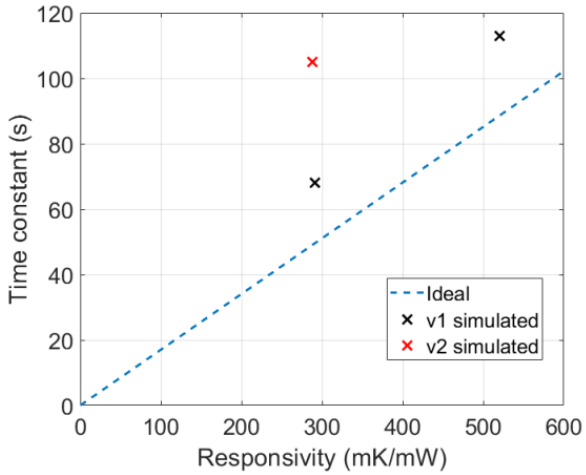


**Figure 3-3**. Simulated time constants at RT as a function of thermal responsivity for fabricated versions (crosses) compared to the minimal (ideal) time constant determined by the heat capacity of the photodiode with size 13 mm x 16 mm x 0.5 mm.

### Assembly of DMD modules and design of trap structure

Metrosert, with input from USN, JV and INRIM, designed and machined a copper trap structure for mounting the two DMD modules in a 45° three-reflection trap, as seen in Fig. 3-4. The DMD modules were attached to copper plate carriers which can be attached by machine screws to the trap structure. The plate position along one axis can be adjusted by 2.5 mm before fastening, to account for relative misalignments between the two assembled DMD modules.

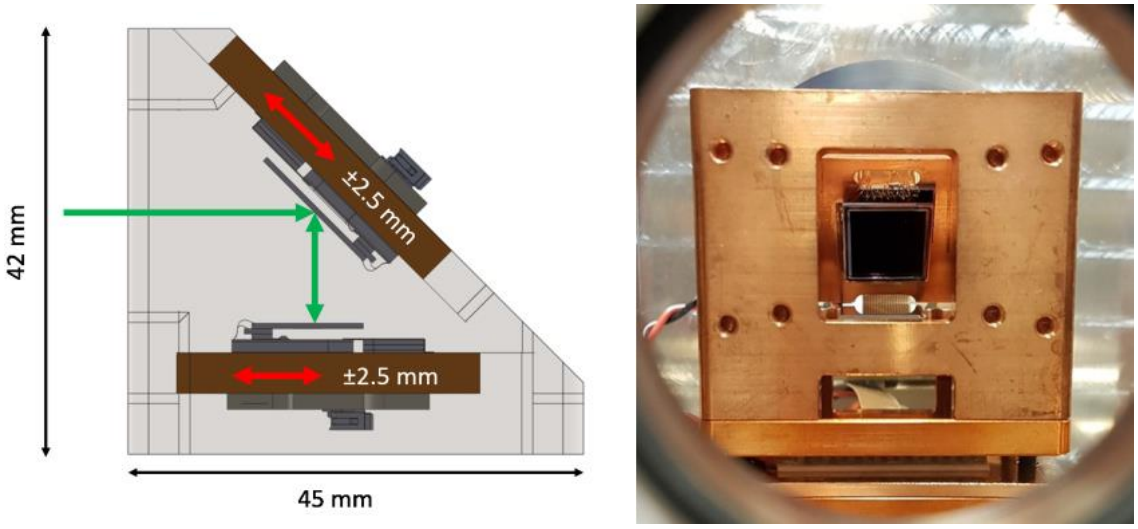


(a) (b)

**Figure 3-4**. (a) Illustration of copper structure for mounting DMD modules in a 45° trap configuration. (b) Photo of an assembled DMD-v1 module in copper trap structure.

### Temperature sensors selection

In addition to optimised heat equivalence, the low uncertainty goals in the project also require optimised signal-to-noise ratio, in both thermal and electrical measurements. Evaluation of various temperature sensors for room and cryogenic temperature was conducted to find the best ones for the purpose, and these were implemented with the chipS·CALe produced photodiodes.

Temperature sensors were characterised in terms of sensitivity, stability and signal-to-noise levels both at room and cryogenic temperatures, by CNAM. At cryogenic temperatures, PT-100, PT-1000 and Cernox CX-1080-SD-HT temperature sensors were tested by CNAM. Based on the results, the Cernox sensor was selected for the cryogenic DMD modules in the bare-chip wire-bondable packaged version.

At room temperature, Adsem (http://www.adsem.com/gpage3.html), PT1000 (Heraeus Nexensos Mfr. No: 3220759532207595) and Semitec (Mfr. No: 103FT1005A5P1) sensors were tested by JV. Based on the results, the Semitec sensor was selected.

### Electronics

The instrumentation and circuitry for the dual-mode measurements were also optimised to reduce the measurement uncertainty to a minimum. The control and measurement instruments used in the two different lab setups at JV – one room temperature setup and one cryogenic setup, are listed in table 3-1. A similar setup was used in dual-mode measurements at INRIM. Figure 3-5 shows a schematic for the room temperature setup. In the cryolab the connection setup was equivalent, using the instruments from the second column in table 3-1.

**Table 3-1**. Control and measurement instruments used in dual-mode measurements at JV, for the room temperature lab and cryolab.

| | Room temperature lab JV | Cryolab JV |
|---|---|---|
| Current reading | Keithley 2002 and transimpedance amplifier | Keithley 2002 and transimpedance amplifier |
| Voltage reading | Keithley 2000 or 2002 | Keithley 2000 |
| Temperature reading | SRS SIM921 AC Resistance bridge | Keysight 3458A |
| Temperature control | Thorlabs TED 350 | Lakeshore 335 |
| Voltage source | Datron 4700<br>PL303QMD | Fluke 5700A |
| Shutter | Uniblitz VCM-01 | Thorlabs SC10 |

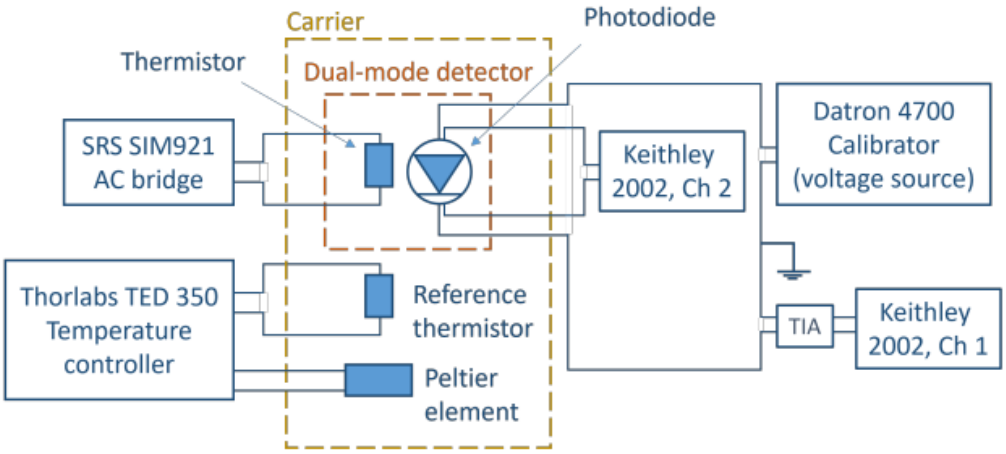


**Figure 3-5**. Diagram showing electrical connections and instruments for the room temperature setup at JV.

Configuration and grounding of the electrical circuit proved to make a considerable difference to the dual-mode measurement result. Figure 3-6 shows a diagram of the final circuit configuration that was used in the project, which is believed to be the most robust configuration against noise and grounding problems.

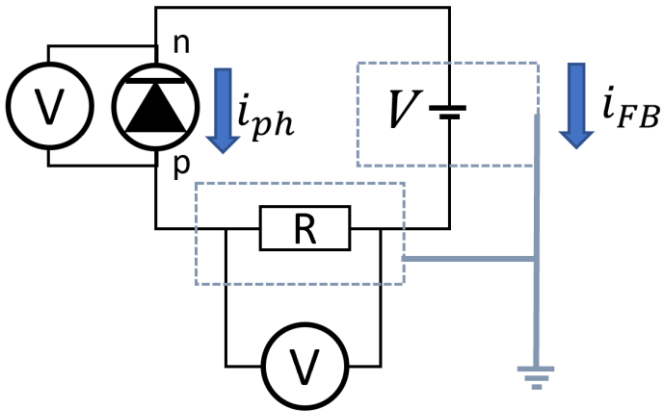


**Figure 3-6**. Ideal configuration of the electrical circuit in the dual-mode measurement. The circuit was grounded through the voltage source.

**Summary**

Two DMD packaging designs (DMD-v1 and DMD-v2) were developed, realised, and successfully tested in dual-mode experiments. COMSOL simulations allowed testing of various parameters to reduce thermal non-equivalence between optical and electrical heating before the optimised design was assembled and tested. USN developed and built the detector modules, Metrosert developed and manufactured a new mechanical three-reflection copper trap structure, and the packaged modules were used in dual-mode measurements both at JV and INRIM. Bi-weekly meetings between all the participating partners for this objective allowed for fruitful discussions in development and testing of the various designs. The objective of developing instrumentation and packaging for self-calibration of photodiodes was successfully met, with two different designs, optimised for operation at room temperature and cryogenic temperature, respectively.

## Objective 4:

*To provide traceability of the self-calibrating photodiodes to the revised SI by measuring the fundamental constant ratio e/h to 1 ppm uncertainty at cryogenic temperatures and to 0.05 % uncertainty at room temperature for wavelengths from 400 nm to 850 nm over a dynamic range from 10 nW to 10 mW*

The purpose of this objective was to perform dual-mode self-calibration measurements with detectors developed under objective 3, both at room temperature and cryogenic temperature, with uncertainties well below the state-of-the-art. There are two independent methods for determining the internal losses of the photodiode:

- Using thermal mode as a reference, in a dual-mode self-calibrating measurement. The internal losses are then found from Equation 3-1.
- Using charge-carrier simulations to fit a model of the photodiode to experimental IV curves and use the fitted model to predict the internal losses.

Combining the two independent methods provides a direct link to the SI through the fundamental constant ratio *e/h*.

**Dual-mode self-calibration at room temperature**

In the dual-mode self-calibration measurement, thermal mode is used as a reference to calibrate the internal losses of the photodiode and is carried out using the method of electrical substitution. In the dual-mode detector we have the option of carrying out the electrical substitution using one of two methods. During the optical heating part, we can either have an open electrical circuit – the open circuit (OC) method, or we can apply an additional electric power at the same time as the optical power is applied – the forward bias (FB) method. The two different methods are illustrated in Fig. 4-1.

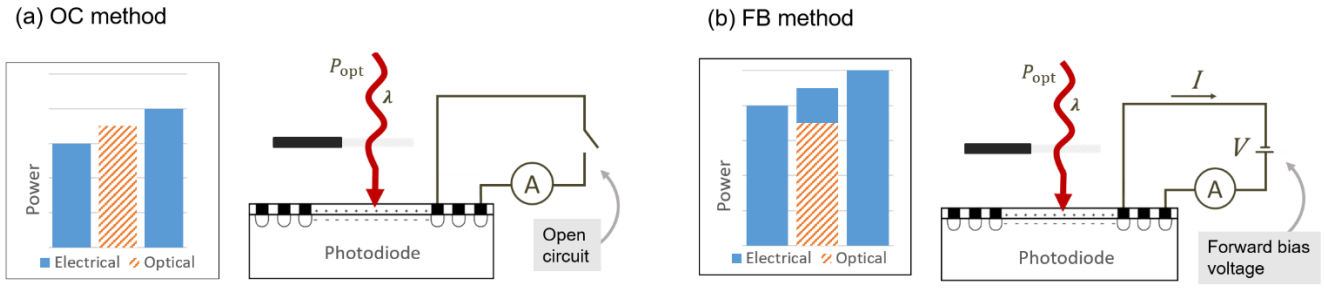


**Figure 4-1**. Schematic showing heating steps for (a) the OC method with open circuit during optical heating, and (b) the FB method with additional electrical heating from forward biasing the photodiode during optical heating.

In our joint publication between JV, USN, Metrosert and INRIM on the room temperature self-calibration (https://doi.org/10.1088/1681-7575/ac6a94), we present dual-mode self-calibration results at 1250 µW optical power at 488 nm, with an expanded standard uncertainty of 400 ppm. The type A contribution was no more than 26 ppm in a 6 hour long measurement sequence. Figure 4-2 shows room temperature results of the dual-mode measurement for different power levels and for the two different measurement methods (OC and FB). Despite the overlap within the measurement uncertainty, a consistent offset can be seen between the two methods. Also, the measured IQD is higher for lower optical power levels and is reduced when increasing the power. A possible reason could be systematic offsets that are more apparent at low power levels.

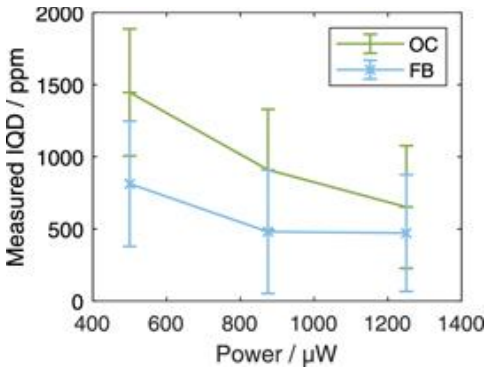


**Figure 4-2**. Measured IQD as a function of absorbed optical power for the two different methods of electrical substitution—OC during optical heating (OC method, green pluses) and FB/electrical heating during optical heating (FB method, blue crosses), using the exponential fit algorithm. The additional electrical heating for the FB method was 100 µW, and error bars show the combined standard uncertainty (k = 1).

Figure 4-3 shows apparent IQD from the dual-mode measurement as a function of beam position on the photodiode, for three different calculation algorithms that are explained in the following section. With an excellent SNR we were able to experimentally verify the modelled change in thermal non-equivalence (solid line) with beam position, resulting in an apparent IQD changing 280 ppm/mm. The grey points in Fig. 4-3 show the IQD when corrected for the simulated non-equivalence.

In beam positions y = 0 and y = 0.5 mm, there is a double measurement point. In each position, measurements were performed before and after the removal of a dust particle on the vacuum chamber window. Removing the dust particle gave a shift in apparent IQD of 130 ppm. Due to scatter of the incoming light from the dust particle, some of the light was absorbed outside the active area of the photodiode. This light produced a thermal signal, but not a photocurrent signal, leading to an over-estimation of the IQD. After the dust particle was removed, the results shifted and aligned nicely along the simulated curve.

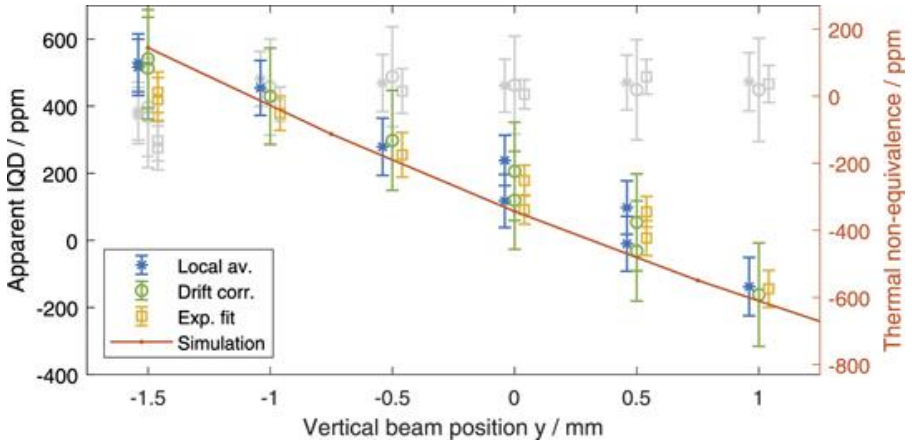


**Figure 4-3**. Apparent IQD (left axis) as a function of beam position on the photodiode with error bars showing propagated type A standard uncertainty. The solid line shows the thermal non-equivalence predicted from simulations (right axis). Measurements were performed using the FB method with optical power of 1250 µW and additional electrical power of 100 µW. Grey points show the IQD when corrected for the simulated non-equivalence.

### Calculation algorithms

To get a good signal-to-noise ratio, the dual-mode detector was thermally stabilised. However, we still observed changes in the background temperature despite the stabilisation, and efforts were made to handle temperature drift in the post-processing of the measurement result. We tested three different calculation algorithms:

1. The local average method involves averaging the heating steps locally around one electrical high or low heating level thereby projecting the optical and electrical measurements to the same time in the measurement sequence.
2. The drift correction method involves a piece-wise linear correction of the temperature signal,
3. The exponential fit method fits the temperature change between the various heating levels to an exponential function and determines the saturation temperature from the fit function. This method was also used to find the thermal time constant.

The results in Fig. 4-3 show good agreement between the three calculation algorithms, suggesting that they can all be used to get a reliable result for the IQD. The exponential fit method has the advantage of lower uncertainty and might be preferential when a clean temperature curve is available. The downside is that the post-processing is more time consuming and slightly more complex to implement than the other two methods.

### Thermal crosstalk between detector modules

When using two dual-mode detector modules in the three-reflection copper trap structure, we observed an unexpected thermal crosstalk between the two modules. Optical heating of the monitor (second) detector was found to cause disturbances in the temperature of the target detector. During optical heating, around 10% of the incoming light is absorbed by the second photodiode. This gives an increase in temperature of the monitor detector module, and this fraction of optical power heats the whole copper trap structure, leading to a temperature drift in the target detector module. This can be seen in Fig. 4-4(a), where each of the heating levels drifts instead of reaching a stable saturation level.

One effective solution to this problem was to electrically heat the monitor detector when the shutter was closed, to maintain a stable temperature of the monitor detector. The temperature signal of the target detector when using this type of electrical compensation can be seen in Fig. 4-4(b).

However, since the dual-mode measurement on the target detector is not dependent on a signal from the monitor detector, we decided to replace the monitor detector with a mirror. The mirror ensured that most of the optical signal was absorbed in the target detector, and we eliminated the crosstalk without having to compensate electrically. The temperature signal when using a mirror in the second detector position is shown in Fig. 4-4(c). The increased reflection from replacing the monitor detector with a mirror did not affect the self-calibration measurement as the measurement is purely relative.

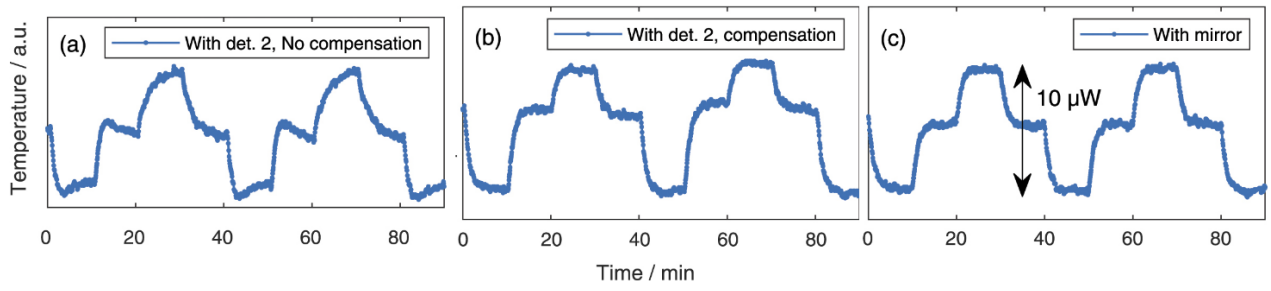


**Figure 4-4.** (a) Temperature signal of the target detector showing drift effects caused by heating of the monitor detector during optical heating. (b) Temperature signal when applying electrical power to the monitor detector during electrical heating, to maintain a constant temperature flow from the monitor detector. (c) Temperature signal when replacing the monitor detector with a mirror. The arrow indicates the power difference between the high and low electrical step.

### Dual-mode measurements at cryogenic temperatures

For improved signal-to-noise ratio, the dual-mode self-calibration was performed at cryogenic temperatures. The aim was to perform a high-accuracy dual-mode measurement providing a link to the SI through the fundamental constant ratio *e/h*, with an uncertainty below 1 ppm. According to thermal modelling, cooling the detector to cryogenic temperatures should improve the heat equivalence to below 1 ppm. In addition, operating the detector at cryogenic temperatures ensures reduced thermal noise, lower heat capacity, increased heat conductivity, lower time constant and better photodiode linearity as compared to room temperature.

This part of the objective was not fully met. However, after characterising the detector at different cryogenic temperatures and improving the electronics and measurement circuits towards a better signal-to-noise ratio, we now have a better understanding of what is needed to reach the aim of 1 ppm uncertainty.

### Icing on photodiode surface

Ice growth on the photodiode surface at low temperatures caused a time variation on the surface reflectance, and hence also on the absorbed optical power. As the resulting power change varies with the same rate for both measurement modes, it will not pose a large problem as long as the time between measurements is short compared to the relative drift.

### Thermal damping

At low temperatures, the temperature signal was initially highly affected by the cryostat's temperature control loop. Influence from the control loop caused oscillations on the temperature signal, as can be seen in Fig. 4-5(a). This was easily solved by passive damping of the system by adding steel plates to the copper structure. The temperature signal after adding the steel plates can be seen in Fig. 4-5(b), and a photo showing the copper structure and the steel plates is shown in Fig. 4-5(c).

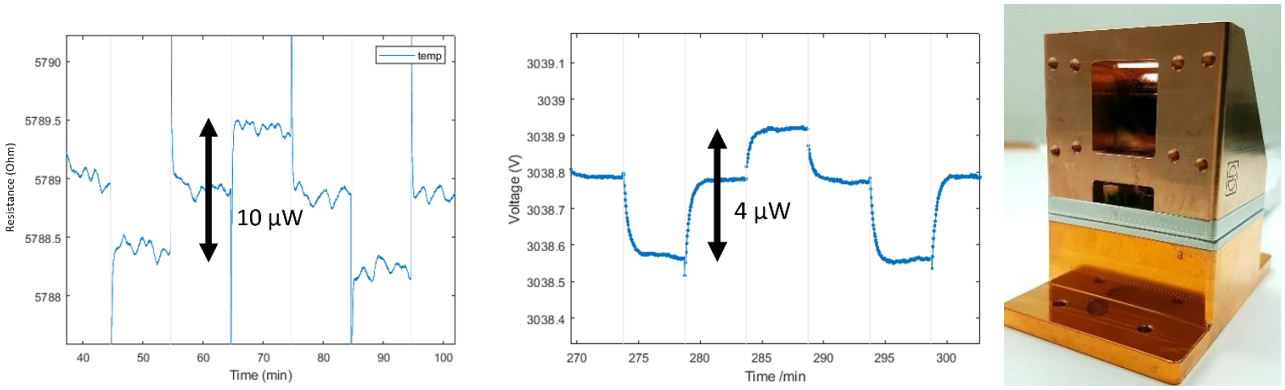


(a) (b) (c)

**Figure 4-5**. Temperature signal of a thermal measurement cycle (a) before and (b) after introducing thermal damping. (c) Copper trap structure showing the steel plates used for thermal damping

### Dual-mode measurements at 80 K and 110 K

Results of the dual-mode self-calibration method performed at 80 K and 110 K are shown in Fig. 4-6. Lower temperatures were also tested, but a temperature dependence on the photocurrent complicated the measurement, and 80 – 110 K was concluded to be the optimum temperature range despite the longer time constant compared to lower temperatures. As for the room temperature results (Fig. 4-2), offsets at lower total power levels can be seen, with a discrepancy between the FB and OC methods. For higher total power the results converge. As for room temperature, this might suggest systematic effects not yet accounted for.

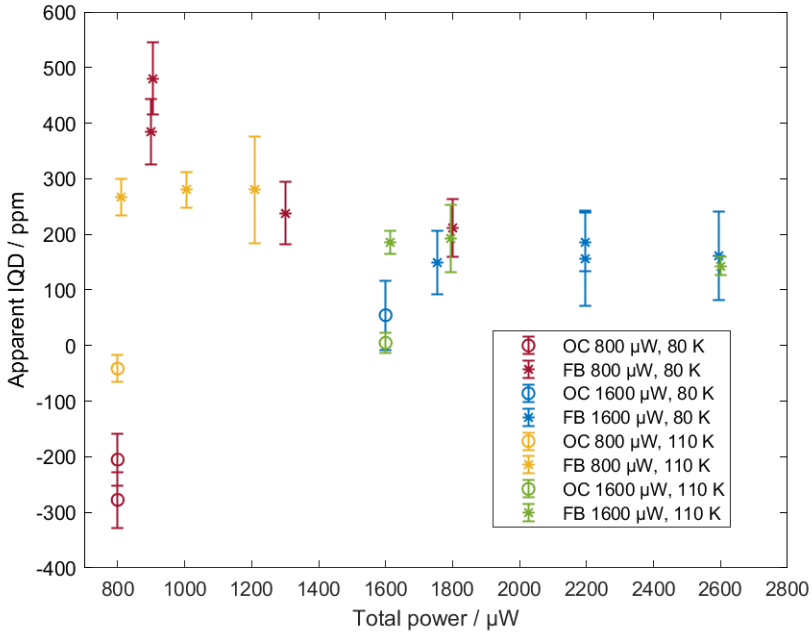


**Figure 4-6**. Estimated IQD from dual-mode measurements at 80 K and 110 K, with optical power of 800 µW and 1600 µW, using the forward bias (FB) method and the open circuit (OC) method. The horizontal axis shows the total amount of heating power, meaning for the FB method optical power plus the additional electrical power.

**Necessary improvements for reaching the 1 ppm uncertainty goal**

Based on our work throughout the project on the cryogenic dual-mode measurements and characterisations, we suggest that the following issues need to be resolved to reduce the uncertainty below the target uncertainty of 1 ppm:

- Ice formation on the photodiode surface: The cryostat should be baked properly to get rid of vapour before cooling. A two-stage temperature control can be used to maintain the dual-mode detector at a higher temperature than the surroundings, to ensure that any remaining water vapour freezes on other surfaces than the photodiode. However, icing does not pose a problem if the measurement time between photocurrent and thermal measurements are low compared to the relative drift in optical power caused by the icing.
- Offset between OC and FB methods: The yet unexplained offset between the measured IQD from the two different methods (OC and FB) should be investigated. The two methods should produce the same result, so a clear understanding of the effect causing this difference is necessary to reduce the measurement uncertainty below 1 ppm.
- Photocurrent stability: By improving the laser stability, the uncertainty of the photocurrent would decrease, as the uncertainty in the electrical measurements are less than 1 ppm and not a limiting factor. Another way to reduce the photocurrent measurement uncertainty is to increase the number of measurements, and a rough estimate indicates that a measurement time of 40 days would reduce the uncertainty on the photocurrent below 1 ppm.
- Temperature stability: A measurement time of 28 days is needed to reduce the uncertainty of the optical power determined from thermal mode below 1 ppm.
- Internal losses: Validations of the charge carrier simulations for estimation of the internal losses, including its uncertainty, are needed to provide the link to the SI through *e/h*.

**Summary**

Self-calibration at room temperature was achieved successfully with a combined standard uncertainty below the goal of 0.05 % for 1250 µW power at 488 nm. At lower power levels there was higher uncertainty and a

discrepancy between the two different methods – with and without additional electrical heating during the optical heating step in electrical substitution. The methods converged at 1250 µW, suggesting that until the low-power discrepancies are explained and fully understood, the self-calibration should be performed at sufficiently high-power levels for the two methods to produce consistent results.

Self-calibration at cryogenic temperatures was not achieved at the proposed uncertainty level of 1 ppm. However, the work in the project has presented us with a broader understanding of low-temperature effects influencing the dual-mode operation, and a suggestion of improvements necessary to reach the 1 ppm goal has been presented. An operational temperature of around 110 K for the SI traceability measurement of *e/h* is suggested. Lower temperatures present thermal dependencies on the photocurrent, which makes these temperatures nonideal despite the lower time constants. Both thermal and electrical measurements and circuitry have been optimised for signal-to-noise ratio and is not considered a limiting factor for the 1 ppm goal.

This objective was fully achieved at room temperature operation, and partly achieved at cryogenic temperatures.

### 18SIB10-RMG1: Application of PQED in the Ultraviolet wavelength range for improved traceability of solar UV irradiance measurements by SFI Davos

The overall aim of the research was to evaluate the applicability of a PQED as a reference for solar ultraviolet radiation, reduce solar irradiance measurements from 2% to 0.5% and learn to use some of the techniques developed in the chipS·CALe project.

SFI Davos operates the World Calibration Centre for solar ultraviolet radiation on behalf of the World Meteorological Organisation. The current traceability chain of spectral solar UV irradiance to the SI is obtained via 1 kW tungsten halogen transfer standard FEL lamps. The stability of these lamps is a limiting factor of the whole measurement process, with an estimated uncertainty of the order of 0.5 %. The PQED will provide an independent assessment of the FEL and 250 W lamp stability and provide a method for monitoring lamp stability with an expected uncertainty of 0.1 %. The RMG aim was to assemble and characterise a PQED device using chipS·CALe silicon photodiodes in the wavelength range from 300 nm to 1050 nm. The work was divided into two tasks:

- Task1: Characterisation of a chipS·CALe silicon PQED device from the ultraviolett to the near infrared wavelength range
- Task2: Determination of degradation effects of the chipS·CALe sililcon PQED after illumination with UV sources.

The work was organised in two one-month stays by SFI Davos researcher at Justervesenet (JV). During the initial stay, the dual-mode PQED was assembled and characterised. Then, the assembled PQED system was illuminated with UV radiation using a HeCd laser at the facilities of PMOD. During the second stay at JV, the PQED characterisation was repeated to determine if the PQED operation was affected by the UV illumination. The overall results were promising and the initial dual-mode measurements at room temperature showed an agreement between photocurrent mode and electrical substitution mode within 200 ppm. While the training and characterisation of the photodiode were successful, the results of the UV degradation are not conclusive due to some problems faced with one of the photodiodes in the initial characterisation period. Assuming that both photodiodes in the PQED were initially identical, there are indications that the photodiode receiving the highest dose of UV radiation changed its response in one of the characterisation methods. The characterisation methods and results are valuable input to the granted 22IEM06 S-CALe Up project where radiation hardness will be tested and improved PQEDs for the ultraviolet spectral range will be developed and manufactured.

# 5 Impact

*(Please leave this section blank. This section will be completed by the EURAMET MSU using text from the final Publishable Summary.)*

# 6 List of publications

*(Please leave this section blank. This section will be completed by the EURAMET MSU using text from the final Publishable Summary.)*

# 7 Contact details

Please delete before you submit your report

## Document Control Page

| | | |
|---|---|---|
| **Document Title:** | EMPIR Contracts<br>Reporting Template 6: Final Publishable Report | |
| **Document Code:** | P-CON-TMP-106 | Version 1.5 |
| **Document Control:** | Approved: Programme Manager | 2021-07-23 |